

Many-flavor Phase Diagram of the $(2 + 1)d$ Gross-Neveu Model at Finite Temperature

Daniel D. Scherer,^{1,2} Jens Braun,^{2,3} and Holger Gies²

¹*Institut für Theoretische Physik, Universität Leipzig, D-04103 Leipzig, Germany*

²*Theoretisch-Physikalisches Institut, Friedrich-Schiller-Universität Jena, Max-Wien-Platz 1, D-07743 Jena, Germany*

³*Institut für Kernphysik (Theoriezentrum), Technische Universität Darmstadt, D-64289 Darmstadt, Germany*

We study the phase diagram of the Gross-Neveu model in $d = 2 + 1$ space-time dimensions in the plane spanned by temperature and the number of massless fermion flavors. We use a functional renormalization group approach based on a nonperturbative derivative expansion that accounts for fermionic as well as composite bosonic fluctuations. We map out the phase boundary separating the ordered massive low-temperature phase from the disordered high-temperature phase. The phases are separated by a second-order phase transition in the $2d$ Ising universality class. We determine the size of the Ginzburg region and show that it scales to zero for large N_f following a powerlaw, in agreement with large- N_f and lattice studies. We also study the regimes of local order above as well as the classical regime below the critical temperature.

I. INTRODUCTION

The Gross-Neveu model [1] in $(2 + 1)$ -dimensions exemplifies many of the intriguing properties of interacting relativistic fermion systems in a planar spacetime. From a theory perspective, it is an ideal laboratory to study the interplay of initially massless fermions with dynamically generated collective excitations. From the viewpoint of applications, the study of effective quantum field theories of low-dimensional Dirac fermions has become a rapidly evolving field in the context of condensed-matter systems like graphene [2], topological band [3–5] and Mott insulators [6], as well as the normal-state behavior of high-temperature superconductors [7, 8].

The Gross-Neveu model in $(2 + 1)$ -dimensions exhibits a quantum phase transition to a phase of broken (discrete) chiral symmetry as a function of the fermionic interaction strength. Despite being perturbatively non-renormalizable, it provides a paradigmatic example for an asymptotically safe theory [9] that is ultraviolet (UV) complete due to the existence of an interacting non-Gaussian renormalization group (RG) fixed point [10]. This fact has been proven to all orders in a $1/N_f$ expansion [11–13] and is supported by lattice simulations [14–16] as well as functional RG studies [17]. The quantum phase transition associated with the RG fixed point has been studied with a variety of techniques [16–27].

Asymptotic safety makes the Gross-Neveu model in $(2 + 1)$ -dimensions a complete theory which is valid on all scales. It also ensures a “perfect” predictive power: once, a single (scale) parameter is fixed, each and every physical observable can be predicted absolutely. This statement extends to all dimensions $2 \leq d < 4$, with the non-Gaussian fixed point merging with the Gaussian fixed point for $d \rightarrow 2$ [17].

From the viewpoint of critical phenomena, the properties of the UV fixed-point control the universal features of the quantum phase transition. Quantitatively, this statement extends to the long-range scaling behavior of the chiral order parameter and/or the correlation length near the phase transition which are both governed by the

critical exponents of the RG fixed point. Also for these critical exponents, the quantitative agreement among the various methods is very satisfactory, see e.g. [16–18, 20].

Whereas the quantum phase transition in the Gross-Neveu model in $2 < d < 4$ dimensions is governed by the coupling strength as a control parameter, many low-dimensional fermion systems can also develop interesting features or even phase transitions as a function of the flavor number N_f , i.e., the number of interacting fermion species. For instance, convincing evidence has been collected for the fact that the $(2 + 1)$ -dimensional Thirring model features chiral symmetry breaking (χ SB) only for flavor numbers below a critical value $N_f < N_{f,\text{cr}}$ [28–31]. A similar behavior is found for fermion systems with gauge interactions such as QED₍₂₊₁₎ [32] or even QCD₍₃₊₁₎ [33]. The latter class of many-flavor theories is currently actively discussed in the context of New Physics scenarios beyond the standard-model of particle physics [34].

In all these cases, non-analytic features as a function of the flavor number N_f occur, limiting the validity region of the large- N_f expansion. The occurrence of a critical flavor number in these models arises from a competition between symmetry stabilizing and destabilizing fluctuations. In this respect, the $(2 + 1)$ -dimensional Gross-Neveu model behaves less dramatically as a function of N_f . Qualitatively, this can be understood from the fact that only one relevant bosonic degree of freedom corresponding to a “radial” \mathbb{Z}_2 mode cannot counterbalance the destabilizing fermion fluctuations at strong coupling. Still, the Gross-Neveu model is not completely structureless as a function of flavor number, as is indicated by several observations: first, in the limit $N_f \rightarrow 0$, fermion interactions are switched off leaving us with a \mathbb{Z}_2 -symmetric universality class of (collective) scalar degrees of freedom and a corresponding Ising-type phase transition. This implies that the Gross-Neveu universality class has to merge with the $3d$ Ising universality class in the limit of small flavor number, approaching a Wilson-Fisher fixed point. From the large- N_f expansion, it is already visible that this merger requires a non-monotonic behavior in the universal quantities. Second, the large-

N_f limit (by definition) merges exactly with mean-field theory which therefore must also hold for the scaling of observables at the finite-temperature transition. On the other hand, simple dimensional reduction suggests that the finite-temperature phase transition is governed by order-parameter fluctuations in the $2d$ Ising universality class which is clearly different from mean-field theory. This mean-field puzzle has first been studied in [35] using lattice simulations, followed by generalized large- N_f expansion techniques in [36]. It turns out that its resolution requires the existence of singularities in the critical exponents in the large- N_f limit.

In the present work, we study the phase diagram of the $(2+1)$ -dimensional Gross-Neveu model as a function of the flavor number and temperature. Because of asymptotic safety, this phase diagram is a pure prediction of the theory once an overall scale parameter is fixed. Our emphasis will be on universal aspects of criticality, as well as near-critical aspects such as local-order phenomena or the width or the critical region. Of particular interest are the approach to the large- N_f limit as well as the expected non-monotonic features at small flavor numbers. All these different aspects can already be studied within a comparatively simple nonperturbative approximation of the functional RG flow, whence we concentrate in the present work on conceptual clarity rather than quantitative precision. As our approximation scheme corresponds to a next-to-leading order result of a derivative expansion of the effective action, higher quantitative precision can be expected from systematic inclusions of higher orders.

Since the physical spin of electrons in condensed-matter applications of the Gross-Neveu model typically plays the role of flavor, the $N_f = 2$ model is phenomenologically most important. For instance, the excitonic [37] or antiferromagnetic instabilities [38] in graphite and graphene, respectively, can be associated with quantum phase transitions falling into this universality class. Also the universal aspects of secondary d - to $d+is$ -wave pairing transitions in nodal d -wave superconductors are expected to be determined by the $N_f = 2$ Gross-Neveu model. Therefore, special N_f -dependent structures of the many-flavor properties which lie near $N_f = 2$ can also exert an influence on physical systems.

This work is organized as follows. In Sect. II, we introduce the model and discuss the relevant symmetries. Section III briefly summarizes the results of a standard mean-field analysis, following earlier works in the literature, see, e.g., Ref. [12]. Section IV is devoted to a functional RG study of the model at next-to-leading order in a derivative expansion. The many-flavor phase diagram at finite temperature and further results are presented in Sect. V. We conclude in Sect. VI and list a number of technically relevant details needed for the RG analysis in the appendix.

II. GROSS-NEVEU MODEL IN $d = 2 + 1$

The classical action of the Gross-Neveu model in d space-time dimensions reads

$$\begin{aligned} S[\bar{\psi}, \psi] &= \int d^d x \left\{ \sum_{j=1}^{N_f} \bar{\psi}_j i \not{\partial} \psi_j + \sum_{i,j=1}^{N_f} \bar{\psi}_i \psi_i \frac{\bar{g}}{2N_f} \bar{\psi}_j \psi_j \right\} \\ &\equiv \int d^d x \left\{ \bar{\psi} i \not{\partial} \psi + \frac{\bar{g}}{2N_f} (\bar{\psi} \psi)^2 \right\}, \end{aligned} \quad (1)$$

where N_f determines the number of fermion flavors. The fermions interact via a four-fermion interaction term with the bare coupling given by \bar{g} of mass dimension $[\bar{g}] = -1$. In our study of the Gross-Neveu model in $d = 2 + 1$, we shall use a reducible four-component ($d_\gamma = 4$) representation for the γ -matrices, as such Dirac spinors appear naturally in the condensed-matter applications of this model, see Refs. [17, 39] for details of our conventions.

The symmetry which is most relevant for the present work is a discrete \mathbb{Z}_2 symmetry with generators given by $\mathbb{Z}_2^5 = \{\mathbb{1}_4, \gamma_5\}$. The nontrivial transformation of the Dirac spinors reads

$$\psi \rightarrow \gamma_5 \psi, \quad \bar{\psi} \rightarrow -\bar{\psi} \gamma_5, \quad (2)$$

implying $\bar{\psi} \psi \rightarrow -\bar{\psi} \psi$ and thus leaving the action (1) invariant. In agreement with the literature, we will refer to this symmetry as a discrete “chiral” symmetry (even though it should rather be viewed as a subgroup of the axial symmetry familiar from $4d$ models.) Note that this transformation acts simultaneously on all flavors.

In addition to this discrete chiral symmetry, the $(2+1)$ -dimensional Gross-Neveu model has a much larger continuous flavor symmetry: using the product of Dirac matrices $\gamma_{35} := i\gamma_3\gamma_5$, we can define the projectors $P_{35,\pm} := (1/2)(\mathbb{1} \pm \gamma_{35})$. For each of the corresponding spinor components $\psi_{i,\pm} := P_{35,\pm} \psi_i$, we can define a separate $U(N_f)_\pm$ flavor rotation, such that the action (1) is invariant under a $U(N_f)_+ \times U(N_f)_-$ continuous symmetry group. However, the latter will not play any relevant role in the following and remains unbroken in the discussed pattern of dynamical symmetry breaking. FRG studies of $3d$ chiral phase transitions with more complicated symmetry-breaking patterns can be found in [31, 40, 41].

Perturbative arguments indicate that the Gross-Neveu field theory in $d = 4$ dimensions is non-renormalizable. This implies that the theory has to be defined with a physical cutoff, introducing – strictly speaking – infinitely many physical parameters that specify the details of the physical regularization. In lower dimensions $2 < d < 4$, the perturbative reasoning is invalidated by the occurrence of a non-Gaussian fixed point in the RG flow that allows to define UV complete renormalized trajectories that emanate from this interacting UV fixed point. This *asymptotic safety* is conceptually reminiscent of UV completeness due to asymptotic freedom with the only difference that the (dimensionless) coupling approaches a

finite fixed-point value in the UV. A detailed analysis [17] shows, that a renormalized trajectory is fully fixed by fixing an overall scale parameter. In $2 < d < 4$, this can, for instance, be done by fixing the dimensionful bare coupling \bar{g}_Λ at an initial scale Λ . For sufficiently strong initial coupling, the system is in the massive chiral-symmetry broken (χ SB) phase such that the scale fixing can also be done by choosing a value for the induced fermion mass m_f .

In the present work, we will always assume that the initial coupling has been chosen super-critically, i. e. the system is in the massive χ SB phase and all observables can be given in units of m_f . To compare different theories, we keep m_f fixed to the same value for all N_f . Incidentally, the critical coupling is directly connected with the non-Gaussian fixed-point coupling, implying a standard relation between the RG fixed-point structure and critical aspects of the chiral quantum phase transition.

In passing, we note that the non-Gaussian fixed point of the four-fermion coupling approaches the non-interacting Gaussian fixed point in the limit $d \rightarrow 2$. In other words, asymptotic safety becomes asymptotic freedom in $d = 2$. Consequently, the phase transition disappears as the system undergoes χ SB for any initial finite value of the coupling with mass generation being associated with “dimensional transmutation”. Even though large parts of the analysis can be done in continuous dimensions, we concentrate on $d = 3$ in the following.

III. MEAN-FIELD ANALYSIS

Let us start by recapitulating a mean-field analysis of the model and its finite-temperature phase transition. Such an analysis has already been performed frequently in the literature, see, e.g., Ref. [12]. We summarize here only the essentials as a preparation for the functional RG analysis. If only fermionic fluctuations are considered as in the following, the mean-field analysis is identical to the large- N_f limit.

We begin by introducing an auxiliary bosonic Hubbard-Stratonovich field $\sigma \sim \bar{\psi}\psi$, leading us to a so-called partially bosonized action:

$$S_{\text{PB}}[\bar{\psi}, \psi, \sigma] = \int_x \left\{ \frac{N_f}{2} \bar{m}^2 \sigma^2 + \bar{\psi} (i\bar{\not{D}} + i\bar{h}\sigma) \psi \right\}. \quad (3)$$

Since the σ field occurs only quadratically, it can be integrated out exactly. This leads us back to the fermionic action (1) if we identify

$$\bar{g} = \frac{\bar{h}^2}{\bar{m}^2}, \quad (4)$$

such that only the ratio $\frac{\bar{h}^2}{\bar{m}^2}$ has a physical meaning at mean-field level. The σ field in Eq. (3) transforms as $\sigma \mapsto -\sigma$ under the discrete chiral transformation. Since its expectation value is directly related to the fermion

condensate $\langle \bar{\psi}\psi \rangle$, it serves as an order parameter for chiral symmetry breaking and renders the fermions massive. From a study of the order parameter for a given N_f we can obtain the critical temperature T_{cr} and analyze the universal critical behavior close to the phase transition, see below.

As the fermions occur only bilinearly in the partially bosonized action (3), they can be integrated out, yielding a nonlocal bosonic effective action for the Gross-Neveu model,

$$S[\sigma] = N_f \int_x \frac{1}{2} \bar{m}^2 \sigma^2 - N_f \text{Tr} \ln(i\bar{\not{D}} + i\bar{h}\sigma). \quad (5)$$

The mean-field/large- N_f approximation is defined by ignoring fluctuations of the σ field, i.e., Eq. (5) defines the full theory at mean-field level. As we expect the ground state to be homogeneous for all temperatures T and flavor numbers N_f , we restrict ourselves to $\sigma = \sigma_0 = \text{const.}$ here and in the following.¹

For constant σ_0 , the effective action boils down to the effective potential, $S[\sigma \rightarrow \sigma_0] = \int_x U(\sigma_0)$, with the ground state satisfying $\partial U(\sigma)/\partial \sigma|_{\sigma_0} = 0$. The solution is found from the variation of the action (5), yielding the gap equation,

$$\sigma_0 = 4 \frac{\bar{h}^2}{\bar{m}^2} \int \frac{d^3 p}{(2\pi)^3} \frac{\sigma_0}{p^2 + \bar{h}^2 \sigma_0^2}. \quad (6)$$

Apart from the trivial solution $\sigma_0 = 0$, we find a non-trivial solution being the global minimum of the effective potential for sufficiently large initial coupling $\bar{g} = \bar{h}^2/\bar{m}^2$. The precise evaluation of Eq. (6) requires, of course, a regularization of the linear UV divergence and a corresponding renormalization of the parameters. Considering a sharp UV cutoff $\Lambda \gg \bar{h}\sigma_0$ for simplicity, we adjust the initial bare coupling $\bar{g} = \bar{h}^2/\bar{m}^2$ at the scale Λ such that the induced fermion mass $\bar{m}_f = \bar{h}\sigma_0$ is kept constant. Ignoring subleading orders in the cutoff, the renormalization condition is given by

$$\bar{m}_f \simeq \frac{2}{\pi} \left(\Lambda - \frac{\pi^2 \bar{m}^2}{2 \bar{h}^2} \right) = \frac{2}{\pi} \Lambda \left(1 - \frac{\pi^2}{2\Lambda \bar{g}} \right), \quad (7)$$

where we can read off the mean-field value of the (non-universal) critical coupling for chiral symmetry breaking, $\bar{g}_{\text{cr}} = \pi^2/(2\Lambda)$ (for a sharp cutoff). The effective potential can be obtained by integrating the gap equation. For $\bar{m}_f \neq 0$, the result is,

$$U(\sigma) = \int_0^\sigma d\sigma' \frac{\partial}{\partial \sigma'} U(\sigma') = \frac{1}{\pi} \left(\frac{1}{3} \bar{h}^3 |\sigma|^3 - \frac{\bar{m}_f}{2} \bar{h}^2 \sigma^2 \right), \quad (8)$$

¹ Inhomogeneous ground states have been found in the GN model in $d = 2$ dimension [42], but only in the presence of a finite chemical potential. Indications for similar phenomena in higher dimensions have also been collected, see, e.g., [43–45].

where all the scheme dependence is cancelled by the corresponding scheme dependence of the relation between the fermion mass \bar{m}_f and the initial couplings [46]. Fixing the physical observable \bar{m}_f , the regularization scheme defines a pair $(\Lambda, \bar{g}(\Lambda))$, such that a different choice for the cutoff Λ is connected with a corresponding adjustment of the initial coupling $\bar{g}(\Lambda)$, such that \bar{m}_f is unaffected.

At finite temperature, the same analysis in the Matsubara formalism requires to replace the momenta $p \rightarrow (\omega_n, \vec{p})$, with the fermionic Matsubara frequencies $\omega_n = (2n+1)\pi T$, and the spatial momenta \vec{p} . Performing the Matsubara sum, the analogue of the gap equation (6) (for $\sigma_0 \neq 0$) reads [12, 14],

$$1 = 4\bar{g} \int \frac{d^2p}{(2\pi)^2} \frac{1}{\sqrt{\vec{p}^2 + \bar{h}^2\sigma^2}} \left[1 - 2n_F \left(\sqrt{\vec{p}^2 + \bar{h}^2\sigma^2} \right) \right], \quad (9)$$

where $n_F(z) = 1/(e^{\beta z} + 1)$ denotes the Fermi distribution function at inverse temperature $\beta = 1/T$. For the system being in the chirally broken phase with fermion mass $\bar{m}_f > 0$ at zero temperature, the gap equation can be reexpressed in terms of the finite-temperature fermion mass,

$$\bar{m}_{f,T} = \bar{m}_f - 2T \ln \left(1 + e^{\bar{m}_{f,T}/T} \right). \quad (10)$$

For fixed zero-temperature fermion mass \bar{m}_f , this transcendental equation can easily be solved numerically for a given temperature, yielding a thermal fermion mass $\bar{m}_{f,T}$ which is monotonically decreasing with temperature. The mean-field critical temperature T_{cr} where $\bar{m}_{f,T=T_{cr}} = 0$ can analytically be read off from Eq. (10),

$$T_{cr} = \frac{\bar{m}_f}{2 \ln 2} \simeq 0.7213 \bar{m}_f. \quad (11)$$

Analogously to Eq. (8), the thermodynamic effective potential can be computed by integrating the gap equation in terms of polylogarithms, yielding [46, 47]

$$\begin{aligned} U(\sigma; T) = & \frac{1}{\pi} \left(\frac{1}{3} \bar{h}^3 |\sigma|^3 - \frac{\bar{m}_f}{2} \bar{h}^2 \sigma^2 \right) \\ & + \frac{2\bar{h}|\sigma|T^2}{\pi} \text{Li}_2 \left(-e^{-\bar{h}|\sigma|/T} \right) \\ & + \frac{2T^3}{\pi} \text{Li}_3 \left(-e^{-\bar{h}|\sigma|/T} \right) + \frac{3T^3}{2\pi} \zeta(3), \end{aligned} \quad (12)$$

where the last term involving the Riemann ζ function has been chosen such that $U(\sigma = 0; T) = 0$. It is instructive to expand the effective potential in powers of the mean field:

$$\begin{aligned} U(\sigma; T) = & \frac{\bar{h}^2 \ln 2}{\pi} (T - T_{cr}) \sigma^2 + \frac{\bar{h}^4}{16\pi T} \sigma^4 \\ & - \frac{\bar{h}^6}{576\pi T^6} \sigma^6 + \dots \end{aligned} \quad (13)$$

Since only even powers of σ appear, the effective potential is analytic in the \mathbb{Z}_2 invariant σ^2 at finite temperature

– in contrast to the $T = 0$ solution, where we observe a $(\sigma^2)^{3/2}$ dependence, cf. Eq. (8).

Finally, we can use these findings to extract thermodynamic critical exponents in the mean-field approximation. The exponents α and β follow straightforwardly from the gap equation (9) and the effective potential Eq. (12), Eq. (13). Expanding Eq. (10) close to T_{cr} to second order in $\bar{m}_{f,T}$, we obtain the relation [12]

$$\bar{m}_{f,T} \simeq 2\sqrt{\bar{m}_f} \sqrt{T_{cr} - T}, \quad (14)$$

from which we can read off the scaling exponent of the order parameter $\beta = 1/2$. Plugging the result for the temperature-dependent ground state into the effective potential, we obtain the free energy $f(T)$ per flavor species and per unit area. Expanding the thermal contribution to fourth order in $\bar{m}_{f,T}$ and differentiating twice with respect to temperature, the specific heat per unit area can be found as [12]

$$c = -T \frac{\partial^2}{\partial T^2} f(T) \Big|_{T=T_{cr}} \simeq \frac{8(\ln 2)^2}{\pi} T_{cr}^2. \quad (15)$$

Since the free energy vanishes in the symmetric phase, this implies $\alpha = 0$, i.e., a jump in the specific heat across the transition. For the exponents δ and γ , the analysis has to be repeated with the inclusion of an external source, whereas the correlation exponent ν and the anomalous dimension η_σ can be derived from the large- N_f limit of the induced bosonic propagator. For instance, the inverse correlation length, corresponding to the induced bosonic mass, $\xi^{-1} = m_\sigma$, turns out to be proportional to the fermion mass, the temperature-scaling of which has been worked out in Eq. (14) above. The correlation exponent $\xi \sim |T_{cr} - T|^{-\nu}$ thus yields the standard mean-field value $\nu = 1/2$. As it should be, also the other exponents yield mean-field values, such that the critical behavior of the Gross-Neveu model in $(2+1)$ dimensions in the large- N_f limit can be summarized by

$$\alpha = 0, \beta = \frac{1}{2}, \gamma = 1, \delta = 3, \nu = \frac{1}{2}, \eta_\sigma = 0. \quad (16)$$

For further details, we refer to [12]. These exponents do not satisfy hyperscaling relations, as can be expected from the fact that bosonic fluctuations which establish such relations are completely suppressed in the large- N_f limit. However, this still raises a question concerning the analyticity of the large- N_f limit: at any finite flavor number, universality suggests that the critical behavior of the thermal phase transition should be governed by order-parameter fluctuations. Since the theory has a \mathbb{Z}_2 symmetry, we expect the phase transition to be in the Ising universality class. This is not reflected by the large- N_f limit given by Eq. (16). Concerning the critical exponents for the transition to the high-temperature phase, the approach to the large- N_f limit must therefore be non-analytic in N_f .

Actually in all of the above-listed mean-field results, the dependence on the flavor number N_f naturally dropped out. Non-trivial flavor information thus requires the inclusion of both fermionic and bosonic fluctuations.

IV. FUNCTIONAL RENORMALIZATION GROUP ANALYSIS

For our nonperturbative study of the many-flavor phase diagram of the Gross-Neveu theory, we employ a functional RG equation for the quantum effective action. For this, we consider a scale-dependent effective action Γ_k , governing the field dynamics at an infrared (IR) scale k . The so-called effective average action Γ_k already comprises all quantum fluctuations from the UV cutoff Λ down to k . In the limit $k \rightarrow 0$, the effective average action is identical to the full quantum effective action, i.e., the 1PI generating functional, whereas it approaches the classical action in the limit $k \rightarrow \Lambda$. The k evolution of Γ_k is determined by the Wetterich equation [48],

$$\partial_t \Gamma_k[\Phi] = \frac{1}{2} \text{STr} \left\{ [\Gamma_k^{(2)}[\Phi] + R_k]^{-1} (\partial_t R_k) \right\}, \quad \partial_t = k \frac{d}{dk}. \quad (17)$$

The quantity $\Gamma_k^{(2)}$ denotes the second functional derivative with respect to the field variable Φ , collecting all fermionic and bosonic fields. The momentum-dependent function R_k is a regulator, suppressing IR modes below a scale k . For reviews of the functional RG adapted to the present context, see Refs. [49–55]. At finite temperature, the effective action is directly related to thermodynamic quantities. For instance, the corresponding effective potential at its minimum corresponds to minus the pressure. In the present work, we intend to study the many-flavor phase diagram in a nonperturbative fashion using our continuum RG approach. For this, we use as an ansatz for the effective action:

$$\Gamma_k[\bar{\psi}, \psi, \sigma] = \int_x \left\{ \frac{N_f}{2} Z_\sigma (\partial_\mu \sigma)^2 + \bar{\psi} (Z_\psi i \not{\partial} + i \bar{h} \sigma) \psi + N_f U(\sigma^2) \right\}, \quad (18)$$

where U denotes the effective potential for the order parameter. The couplings and the wave-function renormalizations Z_σ and Z_ψ are assumed to be scale dependent. This ansatz is related to a systematic derivative expansion at next-to-leading order and has already proved to quantitatively describe the quantum-phase transition at zero temperature [17, 25, 26]. For simplicity, the present ansatz ignores possible anisotropic wave function renormalizations due to the presence of the heat bath, see, e.g., [56].

At the cutoff scale $k = \Lambda$, the initial conditions for the couplings are fixed such that the action (1) is recovered at this scale. This is ensured by the choice

$$Z_{\sigma, \Lambda} \ll 1, \quad Z_{\psi, \Lambda} = 1, \quad \bar{h}_\Lambda^2 = \bar{g}_\Lambda \bar{m}_\Lambda^2, \quad U_\Lambda(\sigma^2) = \frac{1}{2} \bar{m}_\Lambda^2 \sigma^2. \quad (19)$$

From our ansatz (18), we obtain the following flow equation for the dimensionless order-parameter potential $u(\rho) = k^{-d} U(\sigma^2)$:

$$\begin{aligned} \partial_t u = & -du + (d - 2 + \eta_\sigma) u' \rho - 2d_\gamma v_d l_0^{(F)d} (2h^2 \rho; \eta_\psi) \\ & + \frac{1}{N_f} 2v_d l_0^d (u' + 2\rho u''; \eta_\sigma), \end{aligned} \quad (20)$$

where

$$\rho = \frac{1}{2} Z_\sigma k^{2-d} \sigma^2, \quad (21)$$

and the dimensionless renormalized Yukawa coupling

$$h^2 = Z_\sigma^{-1} Z_\psi^{-2} k^{d-4} \bar{h}^2. \quad (22)$$

The corresponding flow for the Yukawa coupling reads,

$$\begin{aligned} \partial_t h^2 = & (d - 4 + 2\eta_\psi + \eta_\sigma) h^2 + \frac{1}{N_f} 8v_d h^4 l_{1,1}^{(FB)d} (2h^2 \kappa, [u'(\kappa) + 2\kappa u''(\kappa)]; \eta_\psi, \eta_\sigma) \\ & - \frac{1}{N_f} (48\kappa u''(\kappa) + 32\kappa^2 u'''(\kappa)) v_d h^4 l_{1,2}^{(FB)d} (2h^2 \kappa, [u'(\kappa) + 2\kappa u''(\kappa)]; \eta_\psi, \eta_\sigma) \\ & - \frac{1}{N_f} 32v_d h^6 \kappa l_{2,1}^{(FB)d} (2h^2 \kappa, [u'(\kappa) + 2\kappa u''(\kappa)]; \eta_\psi, \eta_\sigma), \end{aligned} \quad (23)$$

where the right-hand side is understood to be evaluated at the k -dependent minimum of the effective potential, i.e., $\rho_{\min} = \kappa = 0$ in the symmetric and $\rho_{\min} = \kappa \neq 0$ in the symmetry-broken regime. Here, κ is related to the dimensionless renormalized expectation value of the scalar field,

$$\kappa = \frac{1}{2} \frac{Z_\sigma \sigma_0^2}{k^{d-2}}, \quad (24)$$

satisfying $u'(\kappa) = 0$ in the broken regime. The same conventions apply to the anomalous dimensions

$$\eta_\psi = \frac{1}{N_f} 8 \frac{v_d}{d} h^2 m_{1,2}^{(FB)d} (2h^2 \kappa, [u'(\kappa) + 2\kappa u''(\kappa)]; \eta_\psi, \eta_\sigma), \quad (25)$$

$$\eta_\sigma = 8 \frac{d_\gamma v_d}{d} h^2 \left[m_4^{(F)d} (2h^2 \kappa; \eta_\psi) - 2h^2 \kappa m_2^{(F)d} (2h^2 \kappa; \eta_\psi) \right] + \frac{1}{N_f} 8 \frac{v_d}{d} \kappa (3u''(\kappa) + 2\kappa u'''(\kappa))^2 m_{4,0}^d ([u'(\kappa) + 2\kappa u''(\kappa)], 0; \eta_\sigma). \quad (26)$$

All so-called threshold functions l, m occurring in these flow equations depend on the details of the regulator. Formulas for general regulators as well as explicit expressions for the linear regulator [57] used in this work are given in the appendix. These threshold functions describe the behavior of the regularized 1PI diagrams across mass thresholds and thus describe the decoupling of massive modes from the flow. They also carry the temperature dependence and thus encode also the decoupling of higher Matsubara frequencies as a function of the dimensionless temperature $\tau = 2\pi T/k$. A diagrammatic representation of the flow equations corresponding to our ansatz for the quantum effective action is given in Fig. 1.

V. MANY-FLAVOR PHASE DIAGRAM AND CRITICAL BEHAVIOR

In order to keep the present analysis simple, we solve the flow of the potential in a straightforward polynomial expansion,

$$u(\rho) = \sum_{n=1}^{\infty} \frac{\lambda_{2n}}{n!} (\rho)^n \quad \text{and} \quad u(\rho) = \sum_{n=2}^{\infty} \frac{\lambda_{2n}}{n!} (\rho - \kappa)^n. \quad (27)$$

in the symmetric regime and broken regime ($\kappa > 0$), respectively. Moreover, we ignore higher order couplings with $n \geq 3$. In fact, higher-order approximations, though widely used in the literature, appear to induce artificial instabilities in the present model in a (physically less relevant) temperature interval below $T_{\text{cr}}(N_f)$. We have checked that this approximation does not oversimplify the model by verifying all known limits. For instance, aspects of the large- N_f /mean-field limit such as the critical temperature are reproduced by our simple approximation with an error of $\sim 3\%$ ($T_{\text{cr}} \simeq 0.7439 \bar{m}_f$ in comparison with the exact result $T_{\text{cr}} \simeq 0.7213 \bar{m}_f$, cf. Eq. (11)). We assume that this systematic error is also indicative for the error size at finite N_f .

The following results are obtained from numerically integrating the RG flow in the plane of temperatures and flavor numbers (T, N_f) . Apart from the errors of the numerical routines which are much smaller than the above-mentioned systematic error, we also have to make sure that the initial conditions of the flow lie on the “renormalized trajectory”, i.e., the line of constant physics $(\Lambda, g(\Lambda))$,

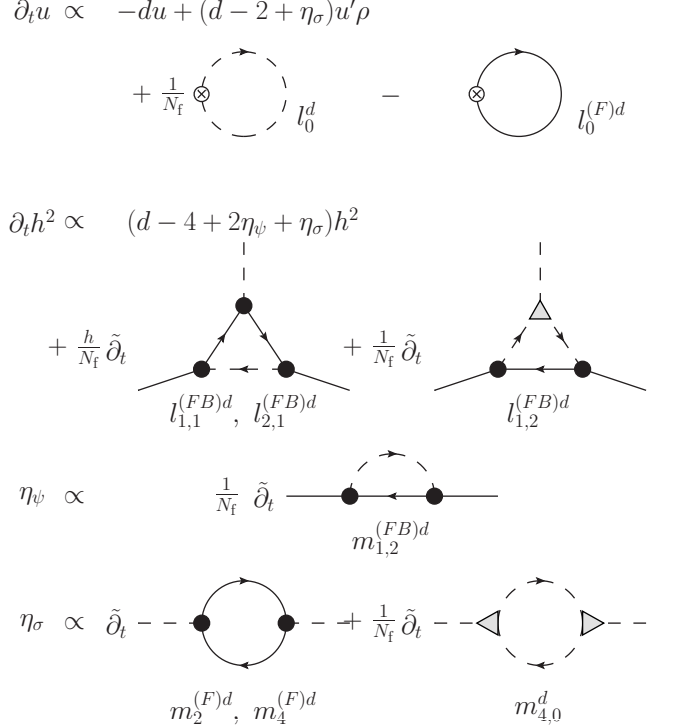


Figure 1: Diagrammatic representation of the flow equations Eq. (21), Eq. (23), Eq. (26) and Eq. (25). The 1PI diagrams represent quantum fluctuations renormalizing the vertex functions at the RG scale k . Full (dashed) lines represent our ansatz for the fermionic (bosonic) propagator modified by a regulator term R_k . Black disks denote the Yukawa vertex, while gray triangles denote vertices $\sim U'''(\sigma)$ which contribute only in the symmetry-broken regime of the flow. Below the 1PI diagrams, the labels (l, m) of the associated threshold functions are given, see appendix for details. The ∂_t -derivative acts on the regulator dependence of the regularized propagators and yields regulator insertions $\partial_k R_k$, as denoted by crossed circles in the flow-diagrams for the effective potential. Note that all diagrams with an internal bosonic line are suppressed by factors of $1/N_f$.

that relates initial conditions for different choices of the cutoff Λ to one and the same physical system in the long-range limit. Moreover, this trajectory must also be on top of or at least sufficiently close to the critical hypersurface emanating from the non-Gaussian fixed point in order to interconnect the long-range limit with the UV

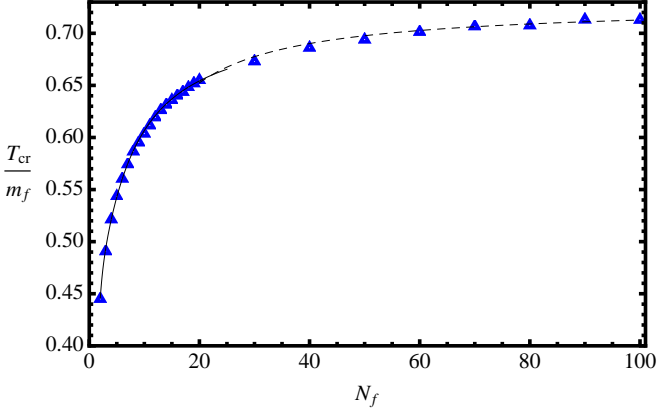


Figure 2: Phase boundary of the Gross-Neveu many-flavor phase diagram as within our ansatz as obtained from set I of initial conditions. We performed temperature scans for flavors $N_f = 1, 2, 3, \dots, 19$ and $N_f = 20, 30, \dots, 100$. Also shown are fits to the phase boundary in the large- N_f and small- N_f region, see Eq. (29) and Eq. (30).

complete theory.² In practice, we keep the UV cutoff fixed at $\Lambda = 100$ a.u. (auxiliary units). Then we choose two different sets of initial parameters for the Yukawa coupling and the mass parameter that are close to the critical manifold. Integrating the flow down towards the IR and expressing all dimensionful quantities in terms of the same scale, such as the renormalized fermion mass,

$$m_f = \frac{1}{Z_\psi} \bar{h} \sigma_0|_{k \rightarrow 0} = \sqrt{2k^2 h^2 \kappa}|_{k \rightarrow 0}, \quad (28)$$

has to lead to quantitatively identical results.³ The first set (set I) of parameters consists of choosing $h_\Lambda = 18.0$ and tuning the bare bosonic mass term $\lambda_{2,\Lambda}$ such that $m_f = 1$ a.u. In the second set (set II), we choose $h_\Lambda = 6.0$ and tune the bare boson mass such that $m_f = 5$ a.u. The initial bosonic wave function renormalization is set to $Z_{\sigma,\Lambda} = 1.0 \times 10^{-3}$, such that the bosonic field is (almost) purely auxiliary at Λ and the corresponding four-fermion vertex is (almost) pointlike. Any difference between the results for these two different sets are due to nonuniversal finite cutoff effects, the influence of irrelevant operators and the corresponding limitations of the truncation. Again, the differences which we find are smaller than the above-mentioned systematic errors.

A typical flow at $T = 0$ starts at $k = \Lambda$ in the symmetric regime, and is then driven by fermion fluctuations into

the broken regime where the flow freezes out, because of mass generation. At finite N_f , the fermion fluctuations are somewhat counterbalanced by the boson fluctuations.

Loosely speaking, finite temperature $T > 0$ favors bosonic fluctuations. This is a generic mechanism as the fermions acquire non-zero thermal masses because of the anti-periodic boundary conditions, whereas this thermal decoupling does not apply to the zeroth Matsubara mode of the bosons. For $0 < T < T_{\text{cr}}$, the zero-temperature condensate generated by the fermions becomes somewhat reduced by the bosonic zeroth Matsubara mode. In this picture, T_{cr} corresponds to the temperature where the bosonic zeroth Matsubara mode is capable of driving the scalar condensate to zero again such that the flow ends again in the symmetric regime. From this point of view, it is also clear that the flow even enters the broken regime at intermediate scales for $T \gtrsim T_{\text{cr}}$, but, of course, ends up in the symmetric regime. This phenomenon of local order is also generic for Yukawa-like systems both in relativistic [56] as well as in non-relativistic systems [58].

Our results for the phase diagram in the (T, N_f) plane up to $N_f = 100$ are shown in Fig. 2. Also shown is a fit to the large- N_f behavior (dashed line)

$$\frac{T_{\text{cr}}(N_f)}{m_f} \simeq 0.72686 - 1.55098 \frac{1}{N_f}, \quad (\text{fit: } N_f = 20, \dots, 100). \quad (29)$$

Here, we did not fix the leading order term (N_f^0) to the exact mean-field value, see Eq. (11). The next-to-leading order (NLO) term $\sim 1/N_f$ is in principle computable with large- N_f techniques [36], though no explicit value is known. The NNLO term has been determined to scale as $(\ln N_f)/N_f^2$, see Ref. [36].

For practical purposes, we also present a fit to the smaller N_f region (solid line),

$$\begin{aligned} \frac{T_{\text{cr}}(N_f)}{m_f} \simeq & 0.695994 - \frac{1.11289}{N_f} + \frac{2.18236}{N_f^2} - \frac{2.43492}{N_f^3} \\ & + \frac{1.04127}{N_f^4}, \quad (\text{fit: } N_f = 2, \dots, 19). \end{aligned} \quad (30)$$

In Fig. 3 as well as in Tab. I, we perform a comparison to existing results in the literature. We compare our FRG results to those from proper-time flows (PTRG) [59] and predictions from two different Monte Carlo simulations (MC) [60, 61]. While [60] provides for a statistical error, an estimate of the systematic errors of each calculation is not available. For instance, the PTRG results are on the one hand obtained from a larger truncation than the present one, but on the other hand do not rely on an exact RG flow [62]. The $N_f = 4$ calculation of [61] provides data for T_{cr}/m_f but no concrete error information. The $N_f = 4$ calculation [60] provides data with a statistical error for T_{cr}/σ_0 which can correspond to T_{cr}/m_f within the conventions of [60] provided a multiplicative renormalization is close to unity. Our results differ from MC [61] and PTRG results by 6% – 8%, which is a deviation slightly larger than our expected systematic error, whereas we find consistency with the MC data of [60]

² Whereas choosing a trajectory exactly on the critical hypersurface is essential for a UV-complete limit, it is numerically not relevant for the long-range physics, as trajectories in the attractive domain of the fixed point are attracted towards the critical hypersurface exponentially fast.

³ Note that at the mean-field level $Z_\psi = 1$, rendering the renormalization factor trivial. In that case the notions of renormalized and unrenormalized mass coincide.

	$N_f = 4$ (MC) [61]	$N_f = 4$ (FRG)	$N_f = 12$ (MC) [60]	$N_f = 12$ (PTRG) [59]	$N_f = 12$ (FRG)
$\frac{T_{cr}(N_f)}{m_f}$	0.49	0.52	0.66 ± 0.05	0.57	0.62

Table I: Comparison of our results (FRG) for $T_{cr}(N_f)$ to those of proper-time renormalization group flows (PTRG) [59] and Monte Carlo simulations (MC) [60, 61]. The conversion of the lattice data of [60] for T_{cr}/σ_0 for $N_f = 12$ to our observable T_{cr}/m_f assumes that a potential multiplicative renormalization constant is close to unity.

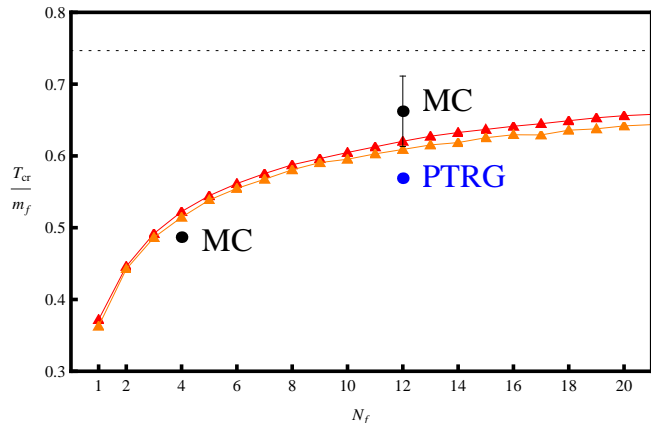


Figure 3: The phase boundary obtained from our flow equations (red triangles corresponding to set I and orange triangles corresponding to set II, respectively) in comparison to available results from proper-time renormalization group (PTRG, $N_f = 12$) [59] and Monte Carlo simulations (MC, $N_f = 4, 12$) [60, 61].

within error bars. On the other hand, our curve appears to be a compromise between the existing results so far, see Fig. 3.

Let us now quantify the phenomenon of local order introduced in the preceding discussion. As mentioned already, even above the critical temperature there is a temperature regime $T_{cr}(N_f) < T < T^*(N_f)$, where the flow first enters the broken regime at intermediate scales k but then re-enters the symmetric regime in the limit $k \rightarrow 0$. This implies that the flow exhibits a (nonuniversal) finite condensate at these intermediate scales which is eventually depleted by the long-range bosonic fluctuations. Identifying $1/k$ with a typical length scale, this intermediate condensate can be interpreted as the existence of local or short-range order on these typical length scales in the system.⁴ Only for higher temperatures $T > T^*(N_f)$, no such local order is observed and the system is in the disordered state on all scales. Our results for $T^*(N_f)$ from numerically solving the flow are depicted in Fig. 4 (dashed line) in comparison with the critical temperature

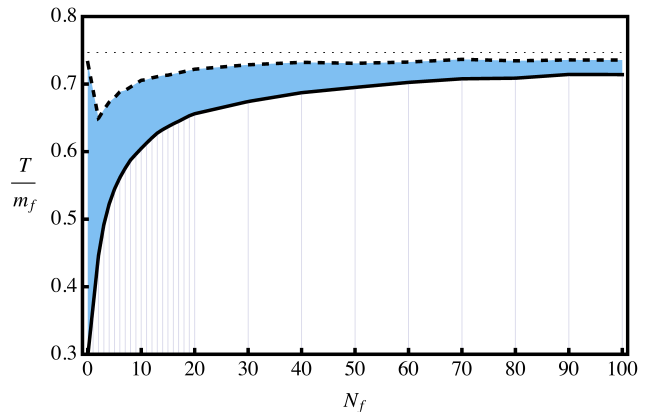


Figure 4: Local order in the Gross-Neveu model: the shaded local-order region is bounded by the critical temperature $T_{cr}(N_f)$ (solid line) and the temperature $T^*(N_f)$ (dashed line) above which the system is in the disordered regime on all scales. In the local-order region, a non-vanishing condensate is found at intermediate k scales, which is ultimately driven to zero by the long-range bosonic fluctuations. Interestingly, the $N_f = 1$ Gross-Neveu model shows an enlarged temperature window compared to theories with $N_f > 1$.

$T_{cr}(N_f)$ (solid line). It is interesting to observe that the $N_f = 1$ Gross-Neveu model shows an enlarged temperature window for local order compared to theories with $N_f > 1$, see Fig. 4. This might be due to the fact that already the UV fixed point potential is closer to the broken regime. The temperature $T^*(N_f)$ lies always below the mean field critical temperature (dotted line). This is only natural, as the local-order phenomenon arises from an interplay of fermionic and bosonic fluctuations whereas the mean-field approximation ignores bosonic fluctuations completely, see our discussion above.

At this point, we would like to add that a RG study of the Gross-Neveu model in a widely-used local potential approximation (i. e. setting $Z_\sigma \equiv 1$ and $Z_\psi \equiv 1$) is not meaningful since it is spoilt by a dramatic parameter dependence. To be more specific, the parameters can be adjusted such that we obtain the same fermion mass in the vacuum for all N_f but the well-known exact result for the critical temperature in the large- N_f limit is nevertheless not reproduced correctly, i. e. it differs, e. g., by a factor of two from the well-known result. This observation can be traced back to the fact that the fixed-point structure of the theory is oversimplified in this approximation.

⁴ For example, the inverse IR regulator scale $1/k$ can be roughly associated with the side length L of the spatial volume in lattice simulations [63].

We now turn to potential non-analyticities of the large- N_f limit. On the one hand, the large- N_f limit discussed in Sect. III *per constructionem* predicts that the finite-temperature phase transition exhibits a mean-field behavior with mean-field critical exponents. On the other hand, general universality arguments suggest that at any finite N_f , the phase transition should be in the $2d$ -Ising universality class, since the scalar order parameter measures the breaking of a discrete \mathbb{Z}_2 symmetry. Also, close to the phase transition, the standard dimensional-reduction mechanism of the Matsubara formalism should be at work, distinguishing the bosonic zero-mode as the driving mode for the approach to criticality.

The RG flow has to be able to resolve the obvious tension between these two apparently contradictory viewpoints. One possibility is that this contradiction is resolved by a non-analytic dependence of the critical phenomena on N_f potentially arising from a failure of the suppression of IR fluctuations with increasing N_f [64]. The other, less dramatic possibility is that the size of the critical region close to the phase transition scales (possibly non-analytically) with increasing N_f to zero, leaving us with the mean-field predictions in the $N_f \rightarrow \infty$ limit. Evidence for the latter possibility has been found in [35] and [36]. In [35], $2d$ -Ising scaling has been verified by measuring the critical exponents very close to the phase transition with lattice simulations for $N_f = 4, 12, 24$. On the other hand, beyond this regime a region obeying mean-field scaling has been identified and the location of the break-down of mean-field scaling in terms of a value for the condensate σ_{MF} has been determined. More precisely, for temperatures $T < T_{cr}$ corresponding to a condensate near $\sigma_0 \gtrsim \sigma_{0,MF}$, mean-field scaling is observed, whereas strong deviations from mean-field scaling and a crossover towards the $2d$ -Ising regime occurs for $\sigma < \sigma_{MF}$, corresponding to temperatures closer to T_{cr} . In Ref. [35], the value of σ_{MF} has been shown to scale as $\sigma_{MF} \sim 1/N_f^{x_{MF}}$. The numerical value for the exponent $x_{MF} \simeq 0.51$ has been measured, nicely corresponding to an analytical estimate $x_{MF} = 1/2$ which was derived from a simple estimate for the validity region of the mean-field approximation [35].

In [36], generalized large- N_f techniques have been used to compute the scaling of a fiducial relative temperature $T - T_{cr}(N_f)$ inside the Ginzburg critical region as a function of N_f , yielding $T - T_{cr}(N_f) \sim 1/N_f^{x_G}$ with $x_G = 1$. It was further argued that a scaling of the mean-field region measured in terms of σ_{MF} with $x_{MF} = 1/2$ and of the Ginzburg region measured in terms of the temperature with $x_G = 1$ is compatible with each other within large- N_f considerations.

In the present work, we go one step further and compute the condensate for a wider range of temperatures, resolving both the mean-field as well as the Ginzburg region. In particular, we directly determine the size of the Ginzburg region around the phase transition. We do so by quantifying the regime where $2d$ -Ising scaling is observed. For consistency reasons, the Ginzburg re-

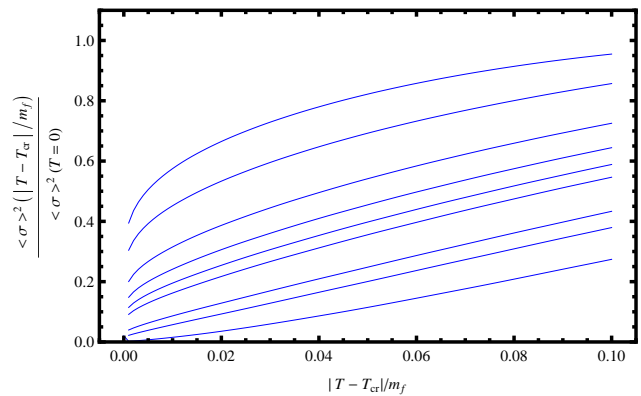


Figure 5: The normalized order parameter squared as a function of temperature close to the phase transition. From top to bottom, the curves correspond to $N_f = 1, 2, 4, 6, 8, 10, 20, 30, 100$. For small N_f , the data is not well described by mean-field theory corresponding to a linear function in this plot. However, as the flavor number increases, the temperature dependence is predominantly linear, as expected from the mean-field scaling with $\beta_{MF} = 1/2$. Deviations from linear scaling occur only upon approaching the critical temperature. As in [35], this suggests an increase of the width of the mean-field scaling region with increasing flavor number.

gion must scale to zero with $N_f \rightarrow \infty$ as fast as or even faster than the validity region of the mean-field approximation. The size and scaling of the Ginzburg region is an important piece of information for experimental searches for the true critical region of the $2d$ order phase transition. In order to identify the Ginzburg region, we use the following strategy: The chiral condensate near the second-order phase transition scales as

$$\langle \sigma \rangle \sim |T - T_{cr}|^\beta, \quad (31)$$

where β in the exact solution should correspond to the exact $2d$ -Ising critical exponent $\beta = 1/8$. The present FRG study indeed boils down to that of a $2d$ scalar \mathbb{Z}_2 -symmetric model near T_{cr} due to dimensional reduction, guaranteeing that we are analyzing the correct universality class. However, our simple truncation is not capable of reproducing the exact Onsager critical exponents. Therefore, we identify the Ginzburg region by identifying the region in the phase diagram where Eq. (31) holds with a value for β which matches that of a $2d$ \mathbb{Z}_2 theory in a σ^4 -truncation at NLO in a derivative expansion (with a linear regulator). For this, we find $\beta_{trunc} = 0.0931$ using completely standard functional FRG techniques [55]. At fixed N_f , a one parameter fit of the form $\langle \sigma \rangle = A|T - T_{cr}|^{\beta_{trunc}}$ with fit parameter A is then applied to a pre-selected region very close to the critical temperature, where the power-law is satisfied by the FRG data. For some flavor numbers, the FRG data is not in perfect agreement with the power-law, possibly due to inaccuracy in the determination of the critical temperature. Our predicted values for the size of the Ginzburg region should thus be taken with some care.

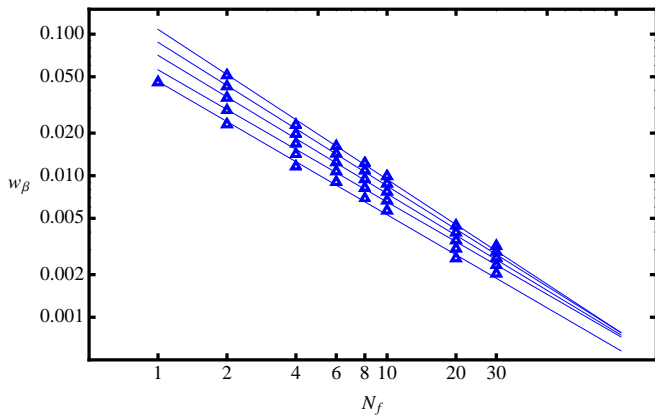


Figure 6: Double-log-plot of the width $w_\beta(N_f)$ (cf. Eq. (32)) of the Ginzburg region close to the finite temperature phase transition as a function of the flavor number N_f . The tolerance criterion increases from bottom to top. The lowest data set corresponds to 2%, while the topmost corresponds to the 6% criterion. Within the Ginzburg region, $2d$ Ising scaling can be observed. The Ginzburg region is suppressed for larger flavor number with a powerlaw $\sim 1/N_f^{x_G}$ with varying from $x_G \simeq 0.93$ to $x_G \simeq 1.06$ (blue lines).

Next, we define the temperature $T_G(N_f)$ characterizing the size of the Ginzburg region by requiring the relative deviation of the one-parameter fit to the FRG data to be less than a few percent inside that region. More precisely, we performed the determination of $T_G(N_f)$ from our data with several criteria corresponding to 2%, 3%, 4%, 5% and finally 6% tolerance.

Repeating the analysis for various N_f , we find that we can fit the corresponding width $w_\beta(N_f)$ of the Ginzburg region scales to a powerlaw

$$w_\beta(N_f) = \left| \frac{T_G(N_f) - T_{cr}(N_f)}{m_f} \right| \sim \frac{1}{N_f^{x_G}}, \quad (32)$$

where the exponent obtained from the fit varies from $x_G \simeq 0.93$ to $x_G \simeq 1.06$ in the range of tolerances from 2% to 6%. This apparent definition dependence of x_G may also originate from the influence of subleading powers of $1/N_f$ which need not be vanishingly small in the fit regime. Still, our result is well compatible with the generalized large- N_f result $x_G = 1$ [36]. In this sense, it is remarkable that this scaling law appears to hold down to rather small values of N_f . A plot of the scaling laws is shown in Fig. 6. Technically, the width becomes more difficult to determine for increasing N_f , as the resolution along the temperature axis has to be finely adapted. In Fig. 6 we show our data in a range from $N_f = 1$ to $N_f = 30$.

Comparing our result for the scaling of the Ginzburg region, $x_G \simeq 1$ with that of [35] for the scaling of the condensate value at the boundary of the mean-field region $x_{MF} \simeq 0.51$, the two different values can be connected by a plausibility argument: our criterion derives

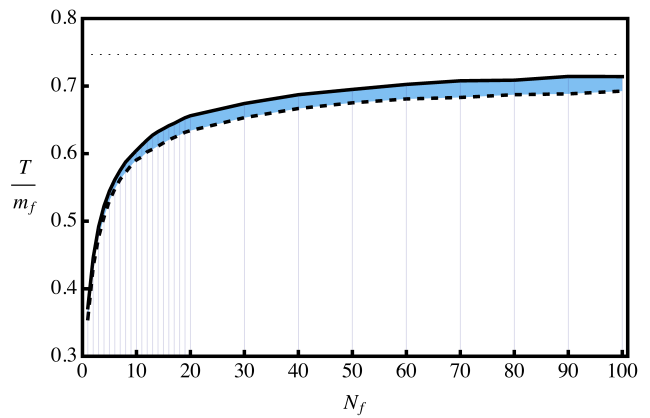


Figure 7: Plot of the classical regime (dashed black) below the phase boundary in the many-flavor phase diagram. The critical region begins where the renormalized thermal mass of the bosonic fluctuations equals temperature, $T^{cl} = m(T^{cl})$. The physics in this region is dominated by the bosonic Matsubara zero mode.

from a quantity scaling with temperature, cf. Eq. (32), whereas [35] studied the scaling of the condensate in the mean-field region. Since mean-field theory predicts a relation between both with an exponent $\beta_{MF} = 1/2$, it is reassuring that the difference between [35] for the scaling exponent of the condensate value at the boundary of the mean-field region x_{MF} and the scaling exponent of the Ginzburg region x_G are separated by an amount on the order of β_{MF} . A formal large- N_f argument [36] also points into the same direction.

Let us conclude this part with a word of caution: Even though the properties within the critical Ginzburg region are universal, the boundary of this region measured in terms of T_G as well as the boundary of the mean-field region may not exhibit the same degree of universality. This is, because T_G is determined by the temperature where the shorter-range thermal fermion and higher-Matsubara boson fluctuations kick in. Such sources of non-universality should even be more pronounced for the location of the boundary of the mean-field region and the corresponding exponent x_{MF} , since the mean-field region is even further apart from the universal critical regime. In fact, we observe an even stronger definition dependence of our results for x_{MF} which nevertheless is roughly of the same size as the lattice value [35].

Finally, let us analyse the size of the so-called *classical regime*, where the dimensional reduction, i.e. the dominance of the bosonic zero mode sets in in the broken phase. Following [35], we define the onset of the classical regime by the value T^{cl} of the temperature where this temperature equals the renormalized bosonic mass $T^{cl} = m(T^{cl})$. In the region $T^{cl} < T < T_{cr}$, the bosonic Matsubara zero mode contributes significantly to the flow. This classical region is shown as a shaded area in Fig. 7. Its width appears to be approximately independent of the flavor number. More quantitatively, we

find that the width $w_{\text{cl}}(N_f)$ of this region, measured in units of the zero-temperature fermion mass, is

$$w_{\text{cl}}(N_f) = \frac{T_{\text{cr}}(N_f) - T^{\text{cl}}(N_f)}{m_f} \simeq \text{const.}, \quad (33)$$

acquires values in the range $w_{\text{cl}} \simeq 0.15 \dots 0.25$ with the smaller values holding for $N_f \lesssim 10$. Therefore, the classical regime remains finite even for $N_f \rightarrow \infty$. This simply reflects the fact that the massless bosonic Matsubara zero mode will always exist near the phase transition even in the presence of an arbitrarily large but finite number of (thermally massive) fermion modes. This phenomenon remains completely invisible in the strict large- N_f limit. This observation indicates that the formal large- N_f limit has to be considered with some care: taking the limit $N_f \rightarrow \infty$ on the level of the path integral does not appear to be equivalent for all physical observables to solving the theory including bosonic fluctuations and then taking the limit $N_f \rightarrow \infty$.

VI. CONCLUSIONS

We have investigated the many-flavor phase diagram of the $(2+1)$ -dimensional Gross-Neveu model at finite temperature. At zero-temperature, the model undergoes a quantum phase transition as a function of the coupling strength, separating a massless from a massive phase. The critical coupling marks a non-Gaussian fixed point which renders the model asymptotically safe, i.e. UV complete despite its perturbative non-renormalizability. As this fixed point has only one relevant direction, all long range observables can in principle be predicted once a single physical scale is fixed. Hence, also the many-flavor finite-temperature phase diagram for the massive model is also a pure prediction of the theory, if expressed, for instance, in units of the vacuum fermion mass m_f . As mass generation as well as symmetry restoration at finite temperature is a non-perturbative process, we have used the functional RG for a determination of various aspects of the phase diagram. In a conceptually comparatively simple framework, the functional RG gives direct access to universal quantities in the critical region near the phase transition as well as non-universal properties. In particular, our predictions for the finite-temperature many-flavor phase boundary can be tested by other non-perturbative approaches, such as lattice Monte-Carlo simulations.

In addition to the phase boundary, we have particularly concentrated on the flavor-number dependence of the phase-diagram regions of (i) local order, (ii) the Ginzburg critical region and (iii) the classical region, all of which correspond to beyond-mean-field or finite- N_f phenomena.

The region of local (or short-range) order at temperatures right above the phase transition characterizes temperature where a finite condensate can be found on intermediate length scales. In addition to possible influences

on the spectral function, an understanding of this region is particularly important for finite-volume studies, since local order can easily be confused with long-range order for too small volumes. It would be indeed interesting to further analyze this question, e. g., by directly employing lattice Monte-Carlo simulations.

The Ginzburg critical region corresponding to the range of temperatures where the phase transition shows universal $2d$ Ising scaling is especially relevant for an understanding of the approach to the large- N_f limit. The non-analytic jump of the critical exponents from $2d$ Ising to mean field at $N_f \rightarrow \infty$ is realized by the size of the Ginzburg critical region vanishing with $1/N_f^{x_G}$. Our result $x_G \simeq 1$ is in accordance with other values in the literature [35, 36].

By contrast, we find that the classical regime, where the dynamics of the bosonic Matsubara zero-mode sets in below T_{cr} , remains finite at any N_f . The existence of this mode cannot be inhibited by a numerical dominance of a large number of flavors. The formal large- N_f limit should therefore be viewed as a pure projection technique onto the fermionic fluctuations rather than a means for quantifying the dynamical prevalence of fluctuations.

With respect to the applications of the Gross-Neveu model in condensed-matter systems, the $N_f = 2$ model is phenomenologically most important. Whereas some quantities such as the many-flavor phase boundary may semi-quantitatively be estimated by higher-order studies in a large- N_f expansion even down to smaller values of N_f , others such as the region of local order show strong variations particularly near $N_f = 2$. This inhibits a general statement about the in-principle applicability or inapplicability of large- N_f expansions for physical phenomena such as instabilities in graphite or graphene, or secondary d - to $d+is$ -wave pairing transitions in nodal d -wave superconductors.

Acknowledgments

The authors thank L. Janssen, F. Karbstein, D. Mesterhazy and M. M. Scherer for useful discussions. JB acknowledges support by the Helmholtz International Center for FAIR within the LOEWE program of the State of Hesse. HG acknowledges support by the DFG under grants Gi 328/5-2 (Heisenberg program). Moreover the authors acknowledge support by the research training group “Quantum and Gravitational Field” (GRK 1523/1) and the research training group FOR 723.

Appendix A: Threshold functions

The regulator dependence of the flow equations is encoded in dimensionless threshold functions which are associated with 1PI diagrams incorporating bosonic and

fermionic fields. In this work we have employed a covariant linear regulator [57] for which the threshold functions at zero temperature are known in closed form, see, e.g., Ref. [26].

At finite temperature, the loop momentum integrals have to be performed by replacing the time-like momentum component by the corresponding fermionic or bosonic Matsubara frequencies. The resulting threshold functions thus acquire a dependence on the dimensionless

temperature parameter $\tau = 2\pi T/k$. For the treatment of loop diagrams with mixed fermionic and bosonic propagators in the loop, we follow the prescription of [66] in order to achieve consistency with the derivative expansion. With the same techniques and definitions as for $T = 0$ and with $v_d^{-1} = 2^{d+1}\pi^{d/2}\Gamma(d/2)$ accounting for Euclidean volume factors, we obtain the following finite temperature threshold functions

$$\begin{aligned}
l_n^d(\tau, \omega_B; \eta_\sigma) &= \frac{\delta_{n,0} + n}{2} \frac{v_{d-1}}{v_d} \frac{\tau}{2\pi} \sum_{n \in \mathbb{Z}} \int_0^\infty dy y^{\frac{d-3}{2}} ((\tau c_{B,n})^2 + y) (\mathcal{G}_\sigma(\tau c_{B,n}, y; \omega_B))^{n+1} \frac{\partial_t(Z_{\sigma,k} r_B)}{Z_{\sigma,k}}, \\
l_n^{(F)d}(\tau, \omega_F; \eta_\psi) &= (\delta_{n,0} + n) \frac{v_{d-1}}{v_d} \frac{\tau}{2\pi} \sum_{n \in \mathbb{Z}} \int_0^\infty dy y^{\frac{d-3}{2}} ((\tau c_{F,n})^2 + y) (\mathcal{G}_\psi(\tau c_{F,n}, y; \omega_F))^{n+1} \times \\
&\quad \frac{(1 + r_F) \partial_t(Z_{\sigma,k} r_F)}{Z_{\psi,k}}, \\
l_{n,m}^{(FB)}(\tau, \omega_F, \omega_B; \eta_\psi, \eta_\sigma) &= -\frac{1}{2} \frac{v_{d-1}}{v_d} \frac{\tau}{2\pi} \sum_{n \in \mathbb{Z}} \int_0^\infty dy y^{\frac{d-3}{2}} \tilde{\partial}_t \{ (\mathcal{G}_\psi(\tau c_{F,n}, y; \omega_F))^n (\mathcal{G}_\sigma(\tau c_{F,n}, y; \omega_B))^m \}, \\
m_2^{(F)d}(\tau, \omega_F; \eta_\psi) &= -\frac{1}{2} \frac{v_{d-1}}{v_d} \frac{d}{d-1} \frac{\tau}{2\pi} \sum_{n \in \mathbb{Z}} \int_0^\infty dy y^{\frac{d-1}{2}} \tilde{\partial}_t \left(\frac{\partial}{\partial y} \mathcal{G}_\psi(\tau c_{F,n}, y; \omega_F) \right)^2, \\
m_4^{(F)d}(\tau, \omega_F; \eta_\psi) &= -\frac{1}{2} \frac{v_{d-1}}{v_d} \frac{d}{d-1} \frac{\tau}{2\pi} \sum_{n \in \mathbb{Z}} \int_0^\infty dy y^{\frac{d-1}{2}} ((\tau c_{F,n})^2 + y) \tilde{\partial}_t \left(\frac{\partial}{\partial y} [(1 + r_F) \mathcal{G}_\psi(\tau c_{F,n}, y; \omega_F)] \right)^2, \\
m_{n,m}^d(\tau, \omega_{B,1}, \omega_{B,2}; \eta_\sigma) &= -\frac{1}{2} \frac{v_{d-1}}{v_d} \frac{d}{d-1} \frac{\tau}{2\pi} \sum_{n \in \mathbb{Z}} \int_0^\infty dy y^{\frac{d-1}{2}} \tilde{\partial}_t \left\{ \left(\frac{\partial}{\partial y} \mathcal{G}_\sigma(\tau c_{B,n}, y; \omega_{B,1}) \right)^{n/2} \times \right. \\
&\quad \left. \left(\frac{\partial}{\partial y} \mathcal{G}_\sigma(\tau c_{B,n}, y; \omega_{B,2}) \right)^{m/2} \right\}, \\
m_{1,2}^{(FB)d}(\tau, \omega_F, \omega_B; \eta_\psi, \eta_\sigma) &= -\frac{1}{2} \frac{v_{d-1}}{v_d} \frac{d}{d-1} \frac{\tau}{2\pi} \sum_{n \in \mathbb{Z}} \int_0^\infty dy y^{\frac{d-1}{2}} \tilde{\partial}_t \left\{ (1 + r_F) (\mathcal{G}_\psi(y; \omega_F)) \left(\frac{\partial}{\partial y} \mathcal{G}_\sigma(y; \omega_B) \right) \right\}.
\end{aligned}$$

where the operator $\tilde{\partial}_t$ is defined as

$$\tilde{\partial}_t|_\sigma = [-2((\tau c_n)^2 + y) r'_B - \eta_\sigma r_B] \frac{\partial}{\partial r_B}, \quad (\text{A1})$$

$$\tilde{\partial}_t|_\psi = [-2((\tau c_n)^2 + y) r'_F - \eta_\psi r_F] \frac{\partial}{\partial r_F}, \quad (\text{A2})$$

depending on whether it acts on bosonic or fermionic propagators. Here, the Matsubara frequencies are encoded by the variable c_n , acquiring the values $c_n = n$ for bosonic terms and $c_n = n + \frac{1}{2}$ for fermionic terms. “Covariant” optimized shape functions now read

$$r_B((\tau c_n)^2 + y) = \left(\frac{1}{[(\tau c_n)^2 + y]} - 1 \right) \Theta(1 - [(\tau c_n)^2 + y]), \quad (\text{A3})$$

$$r_F((\tau c_n)^2 + y) = \left(\sqrt{\frac{1}{[(\tau c_n)^2 + y]}} - 1 \right) \Theta(1 - [(\tau c_n)^2 + y]). \quad (\text{A4})$$

The threshold functions for the linear regulator can be factorized in terms of thermal and vacuum contributions. In the following, full thermal threshold functions and their vacuum counterparts are distinguished by the dependence on

the temperature parameter τ . We find

$$\begin{aligned}
l_n^d(\tau, \omega_B; \eta_\sigma) &= (s_0^d(\tau) - \eta_\sigma \hat{s}_0^d(\tau)) l_n^d(\omega_B; 0), \\
l_n^{(F)d}(\tau, \omega_F; \eta_\psi) &= (s_0^{(F)d}(\tau) - \eta_\psi \hat{s}_0^{(F)d}(\tau)) l_n^{(F)d}(\omega_F; 0), \\
l_{n,m}^{(FB)}(\tau, \omega_F, \omega_B; \eta_\psi, \eta_\sigma) &= \left(\frac{1}{1 + \omega_F} \right)^n \left(\frac{1}{1 + \omega_B} \right)^m \left\{ n (s_0^{(F)d}(\tau) - \eta_\psi \hat{s}_0^{(F)d}(\tau)) l_0^{(F)d}(\omega_F; 0) + \right. \\
&\quad \left. m (s_0^d(\tau) - \eta_\sigma \hat{s}_0^d(\tau)) l_0^d(\omega_B; 0) \right\}, \\
m_2^{(F)d}(\tau, \omega_F; \eta_\psi) &= s_0^{(F)d}(\tau) m_2^{(F)d}(\omega_F; 0), \\
m_4^{(F)d}(\tau, \omega_F; \eta_\psi) &= s_0^{(F)d}(\tau) \left(\frac{1}{1 + \omega_F} \right)^4 + \frac{1 - \eta_\psi}{2} t_4(\tau) \left(\frac{1}{1 + \omega_F} \right)^3 - \\
&\quad \left(\frac{1 - \eta_\psi}{4} t_4(\tau) + \frac{1}{4} s_0^{(F)d}(\tau) \right) \left(\frac{1}{1 + \omega_F} \right)^2, \\
m_{n,m}^d(\tau, \omega_{B,1}, \omega_{B,2}; \eta_\sigma) &= s_0^d(\tau) m_{n,m}^d(\omega_{B,1}, \omega_{B,2}; 0), \\
m_{1,2}^{(FB)d}(\tau, \omega_F, \omega_B; \eta_\psi, \eta_\sigma) &= (s_0^d(\tau) - \eta_\sigma \hat{t}^{(FB)d}(\tau)) m_{1,2}^{(FB)d}(\omega_F, \omega_B; 0, 0).
\end{aligned}$$

The thermal threshold factors are themselves given by the following Matsubara sums

$$\begin{aligned}
s_0^d(\tau) &= \frac{v_{d-1}}{v_d} \frac{d}{d-1} \frac{\tau}{2\pi} \sum_{n \in \mathbb{Z}} \Theta(1 - c_{B,n}^2 \tau^2) (1 - c_{B,n}^2 \tau^2)^{\frac{d-1}{2}}, \\
\hat{s}_0^d(\tau) &= \frac{v_{d-1}}{v_d} \frac{d}{d-1} \frac{\tau}{2\pi} \sum_{n \in \mathbb{Z}} \Theta(1 - c_{B,n}^2 \tau^2) (1 - c_{B,n}^2 \tau^2)^{\frac{d+1}{2}}, \\
s_0^{(F)d}(\tau) &= \frac{v_{d-1}}{v_d} \frac{d}{d-1} \frac{\tau}{2\pi} \sum_{n \in \mathbb{Z}} \Theta(1 - c_{F,n}^2 \tau^2) (1 - c_{F,n}^2 \tau^2)^{\frac{d-1}{2}}, \\
\hat{s}_0^{(F)d}(\tau) &= \frac{v_{d-1}}{v_d} \frac{d}{d-1} \frac{\tau}{2\pi} \sum_{n \in \mathbb{Z}} \Theta(1 - c_{F,n}^2 \tau^2) (1 - c_{F,n}^2 \tau^2)^{\frac{d-1}{2}} \left\{ 1 - |c_{F,n} \tau| {}_2F_1 \left(-1/2, \frac{d-1}{2}; \frac{d+1}{2}; \frac{c_{F,n}^2 \tau^2 - 1}{c_{F,n}^2 \tau^2} \right) \right\} \\
s^d(\tau) &= \frac{v_{d-1}}{v_d} \frac{d}{d-1} \frac{\tau}{2\pi} \sum_{n \in \mathbb{Z}} \Theta(1 - c_{F,n}^2 \tau^2) (1 - c_{F,n}^2 \tau^2)^{\frac{d-1}{2}}, \\
\hat{s}^d(\tau) &= \frac{v_{d-1}}{v_d} \frac{d}{d-1} \frac{\tau}{2\pi} \sum_{n \in \mathbb{Z}} \Theta(1 - c_{F,n}^2 \tau^2) (1 - c_{F,n}^2 \tau^2)^{\frac{d+1}{2}}, \\
\hat{t}^{(FB)d}(\tau) &= \frac{v_{d-1}}{v_d} \frac{d}{d-1} \frac{\tau}{2\pi} \sum_{n \in \mathbb{Z}} \Theta(1 - c_{F,n}^2 \tau^2) (1 - c_{F,n}^2 \tau^2)^{\frac{d+1}{2}} |c_{F,n} \tau|^{-1} {}_2F_1 \left(1/2, \frac{d+1}{2}; \frac{d+3}{2}; \frac{c_{F,n}^2 \tau^2 - 1}{c_{F,n}^2 \tau^2} \right), \\
t_4(\tau) &= \frac{v_{d-1}}{v_d} \frac{d}{d-1} \frac{\tau}{2\pi} \sum_{n \in \mathbb{Z}} \Theta(1 - c_{F,n}^2 \tau^2) \{ c_{F,n}^2 \tau^2 - 1 - 2 \ln(c_{F,n} \tau) \},
\end{aligned}$$

with the hypergeometric function ${}_2F_1(a, b; c; z)$ [65].

In the following, we give closed expressions for the thermal threshold factors, specifically for three spacetime dimensions ($d = 3$), which can be obtained by applying the Poisson resummation formula

$$\sum_{n \in \mathbb{Z}} f(n) = \sum_{l \in \mathbb{Z}} \int_{\mathbb{R}} dq f(q) e^{-2\pi i q l}, \quad (\text{A5})$$

and the identity [67]

$$\text{Li}_n(-z) - (-1)^{n-1} \text{Li}_n(-1/z) = -\frac{(2\pi i)^n}{n!} B_n \left(\frac{\ln z}{2\pi i} + \frac{1}{2} \right), \quad (\text{A6})$$

for $z \notin (0, 1)$ where $B_n(z)$ are Bernoulli polynomials and $\text{Li}_n(z)$ denotes the n th polylogarithm. With

$$\begin{aligned}
\ln(e^{-2\pi i/\tau}) &= -2\pi i + 2\pi i s_F(\tau), \\
\ln(-e^{-2\pi i/\tau}) &= i\pi - \frac{2\pi i}{\tau} + 2\pi i s_B(\tau), \quad (\text{A7})
\end{aligned}$$

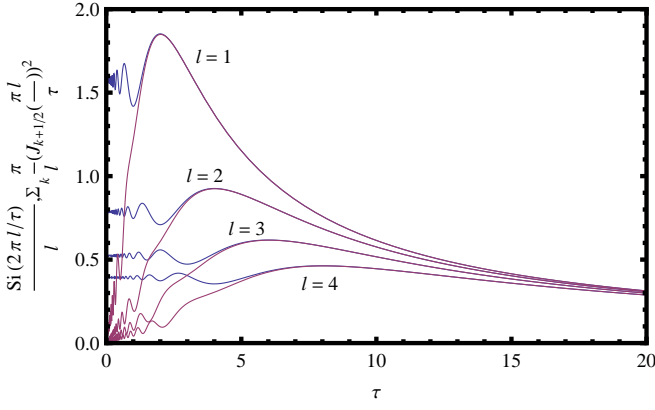


Figure 8: Comparing $\frac{1}{l}\text{Si}\left(\frac{2\pi l}{\tau}\right)$ (blue) and the approximant $\sum_{k=0}^2 \frac{\pi}{l} \left(J_{k+1/2}\left(\frac{\pi l}{\tau}\right)\right)^2$ (magenta) as a function of τ for the Poisson indices $l = 1, 2, 3, 4$. The Poisson resummation over l can be done in closed form for the approximant. The deviation for $\tau \rightarrow 0$ is immaterial since the sine integral enters the thermal threshold factor with a prefactor τ and the flow is stopped at finite τ .

and the definitions of the fermionic and bosonic floor functions [68] $s_F(\tau) = \lfloor \frac{1}{\tau} + \frac{1}{2} \rfloor$, $s_B(\tau) = \lfloor \frac{1}{\tau} \rfloor$, we arrive at

$$\begin{aligned}
s_0^d(\tau) &= \frac{d}{d-1} \frac{v_{d-1}}{v_d} \frac{1}{2\pi} \frac{1}{3} \left(-(\tau + 2\tau s_B(\tau)) (-3 + \tau^2 s_B(\tau) + \tau^2 s_B(\tau)^2) \right), \\
\hat{s}_0^d(\tau) &= \frac{d}{d^2-1} \frac{v_{d-1}}{v_d} \frac{1}{2\pi} \frac{1}{15} \tau (1 + 2s_B(\tau)) \left(15 - \tau^2 (10 + \tau^2) s_B(\tau) + \right. \\
&\quad \left. 2\tau^2 (-5 + \tau^2) s_B(\tau)^2 + 6\tau^4 s_B(\tau)^3 + 3\tau^4 s_B(\tau)^4 \right), \\
s_0^{(F)d}(\tau) &= \frac{d}{d-1} \frac{v_{d-1}}{v_d} \frac{1}{2\pi} \frac{1}{6} \tau s_F(\tau) (12 + (1 + 12)\tau^2 - 4\tau^2 s_F(\tau)^2), \\
\hat{s}_0^{(F)d}(\tau) &= \frac{d}{d-1} \frac{v_{d-1}}{v_d} \frac{1}{2\pi} \frac{1}{12} \left(4s_F(\tau) + (4 + \tau^2) s_F(\tau) - \tau^3 s_F(\tau)^2 - 4\tau^2 s_F(\tau)^3 + \right. \\
&\quad \left. 2\tau^3 s_F(\tau)^4 + \tau^2 (s_F(\tau) - \tau s_F(\tau)^2 - 4s_F(\tau)^3 + 2\tau s_F(\tau)^4) \right), \\
s^d(\tau) &= \frac{d}{d-1} \frac{v_{d-1}}{v_d} \frac{1}{2\pi} \frac{1}{6} \tau s_F(\tau) (12 + \tau^2 - 4\tau^2 s_F(\tau)^2), \\
\hat{s}^d(\tau) &= \frac{d}{d^2-1} \frac{v_{d-1}}{v_d} \frac{1}{2\pi} \frac{1}{120} (\tau s_F(\tau) (240 + 40\tau^2 + 7\tau^4 - 40\tau^2 (4 + \tau^2) s_F(\tau)^2 + 48\tau^4 s_F(\tau)^4)), \\
\hat{t}^{(FB)d}(\tau) &= \frac{d}{d^2-1} \frac{v_{d-1}}{v_d} \frac{1}{2\pi} \frac{2}{3} \tau s_F(\tau) (4 + \tau^2 + \tau^2 s_F(\tau) (-\tau + 2s_F(\tau) (-2 + \tau s_F(\tau)))), \\
t_4(\tau) &= \frac{d}{d-1} \frac{v_{d-1}}{v_d} \frac{1}{2\pi} \left(\frac{1}{6} \tau s_F(\tau) (-12 - \tau^2 + 4\tau^2 s_F(\tau)^2) + \frac{1}{3} \tau (32s_F(\tau) + 2\tau (-12 - \tau^2) s_F(\tau)^2 + \right. \\
&\quad \left. 4\tau^3 s_F(\tau)^4 - \frac{1}{20} \tau (-32s_F(\tau) + 2\tau (40 + 20\tau^2 + 7\tau^4) s_F(\tau)^2 + \right. \\
&\quad \left. 40\tau^3 (-2 - \tau^2) s_F(\tau)^4 + 32\tau^5 s_F(\tau)^6) + \dots \right).
\end{aligned}$$

The expression for $t_4(\tau)$ is only approximate since the Poisson resummation could not be performed analytically.

However, after performing the Poisson integration, the resulting expression contains a sine integral,

which can be expanded in terms of Bessel functions, $\text{Si}(z) = \pi \sum_{k=0}^{\infty} (J_{k+1/2}(\frac{z}{2}))^2$. Above, we expanded to $k = 2$ and cross-checked with numerical evaluation of $t_4(\tau)$, see also Fig. 8. The agreement is satisfactory. In

fact, we have checked that the difference between our approximate expression and the exact result does not lead to significant differences in our results for the phase diagram.

-
- [1] D. J. Gross and A. Neveu, Phys. Rev. D **10**, 3235 (1974).
[2] K. S. Novoselov, A. K. Geim, S. V. Morozov, D. Jiang, M. I. Katsnelson, I. V. Grigorieva, S. V. Dubonos and A. A. Firsov, Nature **438**, 197 (2005), [cond-mat/0509330]
[3] F. Liang, C. L. Kane and E. J. Mele, Phys. Rev. Lett. **98**, 106803 (2007), [cond-mat/0607699].
[4] M. Z. Hasan and C. L. Kane, Rev. Mod. Phys. **82**, 3045 (2010), [arXiv:1002.3895].
[5] X.-L. Qi and S.-C. Zhang, Rev. Mod. Phys. **83**, 1057 (2011), [arXiv:1008.2026].
[6] S. Raghu, X. L. Qi, C. Honerkamp, S.-C. Zhang Phys. Rev. Lett. **100**, 156401 (2008), [arXiv:0710.0030].
[7] A. J. Leggett, Nat. Phys. **2**, 134 (2006).
[8] J. Zaanen, S. Chakravarty, T. Senthil, P. Anderson, P. Lee, J. Schmalian, M. Imada, D. Pines, M. Randeria, C. Varma, M. Vojta, M. Rice, Nat. Phys. **2**, 138 (2006).
[9] S. Weinberg (1976), lectures presented at Int. School of Subnuclear Physics, Ettore Majorana, Erice, Sicily, Jul 23 - Aug 8, 1976.
[10] S. Weinberg (1996), [hep-th/9702027]; S. Weinberg (2009), [arXiv:0903.0568]; M. Niedermaier and M. Reuter, Living Rev. Rel. **9**, 5 (2006); R. Percacci (2007), [arXiv:0709.3851]; O. J. Rosten (2010), [arXiv:1003.1366].
[11] K. Gawedzki and A. Kupiainen, Phys. Rev. Lett. **55**, 363 (1985).
[12] B. Rosenstein, B. J. Warr and S. H. Park, Phys. Rev. Lett. **62**, 1433 (1989); Phys. Rev. D **39**, 3088 (1989).
[13] C. de Calan, P. A. Faria da Veiga, J. Magnen, and R. Seaneor, Phys. Rev. Lett. **66**, 3233 (1991).
[14] S. Hands, A. Kocic and J. B. Kogut, Nucl. Phys. B **390**, 355 (1993).
[15] S. Hands, A. Kocic, and J. B. Kogut, Ann. Phys. **224**, 29 (1993), [hep-lat/9208022].
[16] L. Karkkainen, R. Lacaze, P. Lacock, and B. Petersson, Nucl. Phys. B **415**, 781 (1994), [hep-lat/9310020].
[17] J. Braun, H. Gies and D. D. Scherer, Phys. Rev. D **83**, 085012 (2011), [arXiv:1011.1456].
[18] S. Christofi and C. Strouthos, JHEP **0705**, 088 (2007) [hep-lat/0612031].
[19] G. Gat, A. Kovner, and B. Rosenstein, Nucl. Phys. B **385**, 76 (1992).
[20] J. A. Gracey, Int. J. Mod. Phys. A **9**, 727 (1994), hep-th/9306107.
[21] A. N. Vasiliev, S. E. Derkachov, N. A. Kivel, and A. S. Stepanenko, Theor. Math. Phys. **94**, 127 (1993).
[22] E. Focht, J. Jersak, and J. Paul, Phys. Rev. D **53**, 4616 (1996), [hep-lat/9511005].
[23] T. Reisz (1997), [hep-lat/9712017].
[24] E. Babaev, Phys. Lett. B **497**, 323 (2001), [hep-th/9907089].
[25] L. Rosa, P. Vitale, and C. Wetterich, Phys. Rev. Lett. **86**, 958 (2001), [hep-th/0007093].
[26] F. Hoffing, C. Nowak, and C. Wetterich, Phys. Rev. B **66**, 205111 (2002), [cond-mat/0203588].
[27] H. Sonoda, Prog. Theor. Phys. **126**, 57 (2011) [arXiv:1102.3974 [hep-th]].
[28] M. Gomes, R. S. Mendes, R. F. Ribeiro, and A. J. da Silva, Phys. Rev. D **43**, 3516 (1991).
[29] K. -i. Kondo, Nucl. Phys. B **450**, 251 (1995) [hep-th/9502070].
[30] S. Christofi, S. Hands and C. Strouthos, Phys. Rev. D **75**, 101701 (2007) [hep-lat/0701016]; S. Chandrasekharan and A. Li, Phys. Rev. Lett. **108**, 140404 (2012) [arXiv:1111.7204 [hep-lat]].
[31] H. Gies and L. Janssen, Phys. Rev. D **82**, 085018 (2010) [arXiv:1006.3747 [hep-th]]; L. Janssen and H. Gies, Phys. Rev. D **86**, 105007 (2012) [arXiv:1208.3327 [hep-th]].
[32] R. D. Pisarski, Phys. Rev. **D29**, 2423 (1984); T. W. Appelquist, M. J. Bowick, D. Karabali, and L. C. R. Wijewardhana, Phys. Rev. **D33**, 3704 (1986); P. Maris, Phys. Rev. **D54**, 4049 (1996), hep-ph/9606214; C. S. Fischer, R. Alkofer, T. Dahm, and P. Maris, Phys. Rev. **D70**, 073007 (2004), hep-ph/0407104; E. Dagotto, A. Kocic, and J. B. Kogut, Nucl. Phys. **B334**, 279 (1990); S. J. Hands, J. B. Kogut, L. Scorzato, and C. G. Strouthos, Phys. Rev. **B70**, 104501 (2004), hep-lat/0404013; J. A. Bonnet and C. S. Fischer, Phys. Lett. B **718**, 532 (2012) [arXiv:1201.6139 [hep-ph]].
[33] W. E. Caswell, Phys. Rev. Lett. **33**, 244 (1974); T. Banks and A. Zaks, Nucl. Phys. **B196**, 189 (1982); V. A. Miransky and K. Yamawaki, Phys. Rev. **D55**, 5051 (1997), hep-th/9611142; T. Appelquist, J. Terning, and L. C. R. Wijewardhana, Phys. Rev. Lett. **77**, 1214 (1996), hep-ph/9602385; F. Sannino and J. Schechter, Phys. Rev. **D60**, 056004 (1999), hep-ph/9903359; H. Gies and J. Jaeckel, Eur. Phys. J. **C46**, 433 (2006), hep-ph/0507171; D. D. Dietrich and F. Sannino, Phys. Rev. D **75**, 085018 (2007) [hep-ph/0611341]; J. Braun and H. Gies, Phys. Lett. **B645**, 53 (2007), hep-ph/0512085; J. Braun and H. Gies, JHEP **06**, 024 (2006), hep-ph/0602226; H. Terao and A. Tsuchiya (2007), 0704.3659; S. Catterall and F. Sannino, Phys. Rev. **D76**, 034504 (2007), 0705.1664; T. Appelquist, G. T. Fleming, and E. T. Neil, Phys. Rev. Lett. **100**, 171607 (2008), 0712.0609; A. Deuzeman, M. P. Lombardo, and E. Pallante, Phys. Lett. **B670**, 41 (2008), 0804.2905; A. Deuzeman, M. P. Lombardo, and E. Pallante (2009), 0904.4662; T. Appelquist, G. T. Fleming, and E. T. Neil, Phys. Rev. **D79**, 076010 (2009), 0901.3766; Z. Fodor, K. Holland, J. Kuti, D. Negradi, and C. Schroeder (2009), 0911.2463; E. Pallante (2009), 0912.5188; T. DeGrand (2010), 1010.4741; J. Braun, C. S. Fischer and H. Gies, Phys. Rev. D **84**, 034045 (2011) [arXiv:1012.4279 [hep-ph]]; K. Miura, M. P. Lombardo and E. Pallante, Phys. Lett. B **710**, 676 (2012) [arXiv:1110.3152 [hep-lat]]; K. Miura and M. P. Lombardo, arXiv:1212.0955 [hep-lat].
[34] S. Weinberg, Phys. Rev. **D19**, 1277 (1979); B. Holdom,

- Phys. Rev. **D24**, 1441 (1981); D. K. Hong, S. D. H. Hsu, and F. Sannino, Phys. Lett. **B597**, 89 (2004), [hep-ph/0406200]; F. Sannino and K. Tuominen, Phys. Rev. **D71**, 051901 (2005), [hep-ph/0405209]; F. Sannino, Acta Phys. Polon. **B40**, 3533 (2009), 0911.0931.
- [35] J. B. Kogut, M. A. Stephanov and C. G. Strouthos, Phys. Rev. D **58**, 096001 (1998), [hep-lat/9805023].
- [36] S. Caracciolo, B. M. Mognetti and A. Pelissetto, PoS LAT **2005**, 187 (2006) [hep-lat/0509063]; Nucl. Phys. B **741**, 421 (2006) [hep-lat/0601018]; B. M. Mognetti, hep-lat/0703020 [HEP-LAT].
- [37] D. V. Khveshchenko, Phys. Rev. Lett. **87**, 246802 (2001), [cond-mat/0101306].
- [38] I. F. Herbut, Phys. Rev. Lett. **97**, 146401 (2006), [cond-mat/0606195].
- [39] D. D. Scherer, “Low-dimensional chiral physics: Gross-Neveu universality and magnetic catalysis”, PhD thesis, Jena (2012).
- [40] H. Gies, L. Janssen, S. Rechenberger and M. M. Scherer, Phys. Rev. D **81**, 025009 (2010) [arXiv:0910.0764 [hep-th]].
- [41] D. Mesterhazy, J. Berges and L. von Smekal, arXiv:1207.4054 [cond-mat.str-el].
- [42] V. Schon and M. Thies, Phys. Rev. D **62**, 096002 (2000), [hep-th/0003195]; M. Thies and K. Urlichs, Phys. Rev. D **67**, 125015 (2003), [hep-th/0302092]; M. Thies, Phys. Rev. D **69**, 067703 (2004), [hep-th/0308164]; G. Basar and G. V. Dunne, Phys. Rev. Lett. **100**, 200404 (2008), [arXiv:0803.1501]; G. Basar and G. V. Dunne, Phys. Rev. D **78**, 065022 (2008), [arXiv:0806.2659].
- [43] D. Nickel, Phys. Rev. D **80**, 074025 (2009), [arXiv:0906.5295].
- [44] S. Carignano and M. Buballa, Phys. Rev. D **86**, 074018 (2012) [arXiv:1203.5343 [hep-ph]].
- [45] T. Kojo, Y. Hidaka, K. Fukushima, L. D. McLerran and R. D. Pisarski, Nucl. Phys. A **875**, 94 (2012) [arXiv:1107.2124 [hep-ph]].
- [46] F. Cooper and V. M. Savage, Phys. Lett. B **545**, 307 (2002), [hep-ph/0208057].
- [47] H. Caldas and R. O. Ramos, Phys. Rev. B **80**, 115428 (2009), [arXiv:0907.0723].
- [48] C. Wetterich, Phys. Lett. B **301**, 90 (1993).
- [49] J. Braun, J. Phys. G **39**, 033001 (2012), [arXiv:1108.4449].
- [50] K. Aoki, Int. J. Mod. Phys. B **14**, 1249 (2000).
- [51] P. Kopietz, L. Bartosch, and F. Schütz, Introduction to the functional renormalization group (Springer Verlag, Berlin, 2010).
- [52] W. Metzner, M. Salmhofer, C. Honerkamp, V. Meden, and K. Schonhammer, [arXiv:1105.5289].
- [53] J. M. Pawłowski, Ann. Phys. **322**, 2831 (2007), [hep-th/0512261].
- [54] H. Gies, Lect. Notes Phys. **852**, “Renormalization Group and Effective Field Theory Approaches to Many-Body Systems” ed. by A. Schwenk, J. Polonyi (2012), [hep-ph/0611146].
B. Delamotte (2007), [cond-mat/0702365].
- [55] J. Berges, N. Tetradis and C. Wetterich, Phys. Rept. **363**, 223 (2002), [hep-ph/0005122].
- [56] J. Braun, Phys. Rev. D **81**, 016008 (2010), [arXiv:0908.1543].
- [57] D. F. Litim, Phys. Lett. B **486**, 92 (2000), [hep-th/0005245]; D. F. Litim, Int. J. Mod. Phys. A **16**, 2081 (2001), [hep-th/0104221]; D. F. Litim, Phys. Rev. D **64**, 105007 (2001), [hep-th/0103195].
- [58] S. Diehl, H. Gies, J. M. Pawłowski and C. Wetterich, Phys. Rev. A **76**, 021602 (2007), [cond-mat/0701198]; S. Diehl, S. Floerchinger, H. Gies, J. M. Pawłowski and C. Wetterich, Annalen Phys. **522**, 615 (2010) [arXiv:0907.2193 [cond-mat.quant-gas]]; I. Boettcher, J. M. Pawłowski and S. Diehl, Nucl. Phys. Proc. Suppl. **228**, 63 (2012) [arXiv:1204.4394 [cond-mat.quant-gas]].
- [59] P. Castorina, M. Mazza, and D. Zappala, Phys. Lett. B **567**, 31 (2003), [hep-th/0305162].
- [60] S. Hands, Nucl. Phys. A **642**, 228 (1998), [hep-lat/9806022].
- [61] J. B. Kogut and C. G. Strouthos, Phys. Rev. D **63**, 054502 (2001), [hep-lat/9904008].
- [62] D. F. Litim and J. M. Pawłowski, Phys. Rev. D **66**, 025030 (2002) [hep-th/0202188].
- [63] J. Braun, B. Klein and H. -J. Pirner, Phys. Rev. D **71**, 014032 (2005) [hep-ph/0408116]; J. Braun, B. Klein and P. Piasecki, Eur. Phys. J. C **71**, 1576 (2011) [arXiv:1008.2155 [hep-ph]].
- [64] S. Chandrasekharan and C. G. Strouthos, Phys. Rev. Lett. **94**, 061601 (2005) [hep-lat/0410036].
- [65] I. S. Gradshteyn and I. M. Ryzhik, Table of integrals, series, and products (Jeffrey, Alan (ed.), Academic Press, 2000).
- [66] J. Braun, Eur. Phys. J. C **64**, 459 (2009), [arXiv:0810.1727].
- [67] L. Lewin, “Polylogarithms and Associated Functions” (Elsevier Science Ltd., 1981).
- [68] F. Synatschke, J. Braun and A. Wipf, Phys. Rev. D **81**, 125001 (2010), [arXiv:1001.2399].